Intermolecular interactions of nanocrystalline alkali-silica reaction products under sorption

Tulio Honorio, Ornella Chemgne Tamouya, Zhenguo Shi, Alexandra Bourdot

Intermolecular interactions of nanocrystalline alkali-silica reaction products under sorption

Tulio Honorio[a,*], Ornella M. Chemgne Tamouya[a], Zhenguo Shi[b], Alexandra Bourdot[a]

[a] *Université Paris-Saclay, ENS Paris-Saclay, CNRS, LMT - Laboratoire de Mécanique et Technologie, 94235, Cachan, France*
[b] *Laboratory for Concrete & Construction Chemistry, Swiss Federal Laboratories for Materials Science and Technology (Empa), 8600 Dübendorf, Switzerland*

Abstract

There is no consensus on the physical origin of alkali-silica reaction (ASR) damage in concrete. Atomic-level detail on the intermolecular interactions of ASR products with water is critical to understand the development and to propose solutions to mitigate ASR. We combine molecular dynamics and Monte Carlo simulations to model ASR products under sorption. The hydration of shlykovite, a naturally occurring phyllosilicate structurally similar to ASR products, is analyzed with atomic-level detail. Sodium and potassium, the most relevant alkali in ASR, are considered as charge balancing cations in shlykovite. Intra- and inter-layer water content and volume remain stable under sorption at ambient pressure, which corroborates that swelling of crystalline products cannot be at the origin of ASR damage. Also, we provide the effective interactions of Na- and K-shlykovite under water-saturated conditions. These potentials of mean force can be used in mesoscale simulations to test other mechanisms of ASR damage.

Keywords: Molecular Dynamics; Grand Canonical Monte Carlo simulations; Shlykovite; Swelling Thermodynamics; Adsorption.

*Corresponding author
Email address: tulio.honorio-de-faria@ens-paris-saclay.fr (Tulio Honorio)

Highlights

- Na- and K-shlykovite are molecular modeled for the first time
- Water content and volume of shlykovite remain stable for RH ranging from 20 to 100%
- Na- and K-shlykovite exhibits significant differences in volume and water content
- The effective interactions of Na- and K-shlykovite provided can be used in mesoscale simulations.

1. Introduction

Alkali-silica reaction (ASR) is a deleterious process involving the alkaline encountered in the pore solution of cement-based materials (mainly, sodium and potassium cations) and the disordered silica in aggregates (e.g. [1, 2]). The formation of ASR products leads to cracking and degradation of the mechanical properties of concrete, reducing the service life of the affected structures [3]. ASR cracking also affects the sealing capacity, a performance specification that is critical in energy production infrastructures such as dams, nuclear power plants, oil wells, and nuclear waste disposal strictures on concrete.

Since ASR has been first described in 1940 [4], fundamental questions remain open regarding the physical origin of the expansive behavior, the structure, and the properties of the ASR products. We still know relatively little about mechanisms leading to ASR development and damage. Swelling at the molecular scale has been for decades evoked as the mechanism driving ASR damage.

Molecular simulations have been extensively used to reveal, with atomic-level detail, the propensity of phyllosilicates to swell [5, 6, 7, 8, 9], according to specific ion effects and possible isomorphic substitutions [10, 11, 12]. To date, only a few studies have coped with the molecular modeling of ASR products. Kirkpatrick et al. [13] performed molecular dynamics (MD) simulations using kanemite

structure to represent nano-crystalline ASR products and ClayFF [14] to model the interactions. Their results suggest that water ingress in ASR products is limited at the molecular scale, which corroborates the experimental evidence [15, 16]. However, recent studies show that kanemite molecular structure is not equivalent to the structure of ASR products found in concrete [15, 17, 18]. A recent experimental study [15] shows that crystalline ASR products are similar to the naturally occurring mineral shlykovite ($KCa[Si_4O_9(OH)].3H_2O$]) [19], with isomorphic substitutions of potassium by sodium taking place according to the composition of the pore solution. Experiments on Na- and K-shlykovite reports no swelling under sorption [15]. In this case, other mechanisms should be favored to explain ASR damage.

In this work, we carry out classical molecular dynamics and Monte Carlo simulations to dissect the intermolecular interactions of crystalline ASR products with water. To the best of the author's knowledge, this is the first time that shlykovite is modeled at the molecular scale. Sodium and potassium (that are among the main alkali found in cement-based materials pore solutions [20, 21]) substitutions in shlykovite are considered. The structure obtained from the molecular simulation are compared to experimental data on ASR products. Hydration and isosteric energies of adsorption are computed for systems controlled on the water content. Hybrid GCMC-NσT simulations are carried out to investigate the stability under sorption for stress-controlled systems. Hybrid GCMC-NVT simulations are carried out to obtain the effective interactions under liquid water-saturated conditions (relative humidity of 100%) and 296 K. These effective interactions can be used as input in future work tackling the mesoscale texture formation and crystallization-induced pressure in ASR product formation.

2. Molecular models and methods

2.1. Atomic structure

We adopt the atomic structure of shlykovite as reported by Zubkova et al. [19]. Shlykovite is a monoclinic (space group $P2_1/c$) phyllosilicate [19, 22]. Figure 1 shows a snapshot of Na-shlykovite (i.e. a structure in which all K atoms are substituted by Na atoms). The main layer is composed of silicate sheets sandwiching a calcium and water (intra-)layer. The main solid layer is stacked along *c*-axis. The silicate sheet exhibits silanol groups projected outwards the main layer forming a structure with channels similar to that observed in other phyllosilicates such as tobermorite [9]. The interlayer space is occupied by water molecules. Potassium and sodium cations are located within these channels, similarly to inner-sphere complexes formed by calcium counterions in tobermorite channels [9]).

2.2. Force fields

We reparametrize ClayFF [14] to model the interactions in shlykovite. The total energy of the system is modeled by a sum of the contributions from the short-range interactions (van der Waals forces and steric repulsion), the electrostatic (Coulombic) interactions, and the 2- and 3-body interactions (bond and angle, respectively):

$$U^{Tot} = U^{VdW} + U^{Coul} + U^{Bond} + U^{Angle} \tag{1}$$

The nonbonded interactions are described by the Lennard-Jones (12-6) potential:

$$U^{VdW} = \sum_{i \neq j} 4\epsilon_{LJ} \left[\left(\frac{\sigma_{LJ}}{r_{ij}} \right)^{12} - \left(\frac{\sigma_{LJ}}{r_{ij}} \right)^{6} \right] \tag{2}$$

where r_{ij} is the distance between the particles i and j; ϵ_{LJ} and σ_{LJ} are empirical parameters. In the following, these parameters are defined only for the same

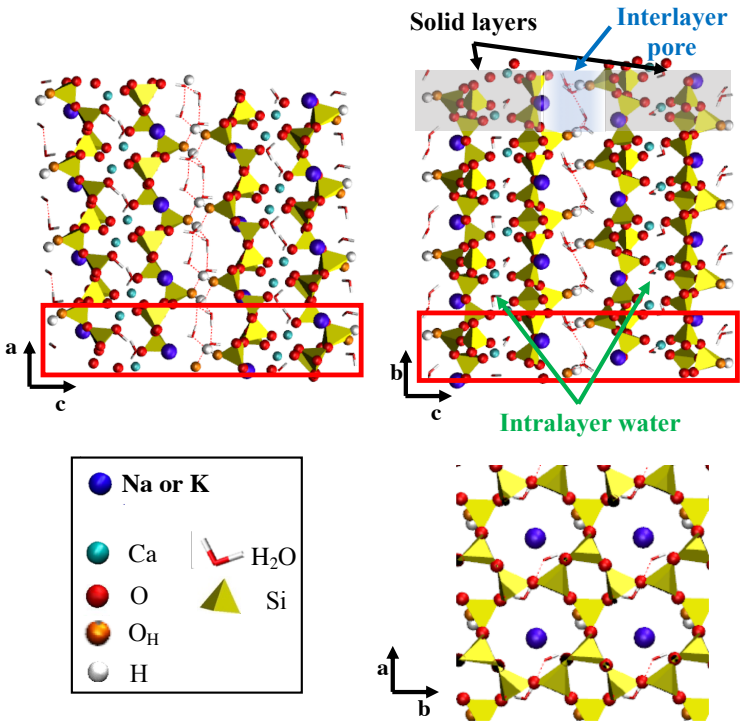

Figure 1: Snapshot of Na-shlykovite for a number of water molecules n=3 (per $Ca[Si_4O_9(OH)]$), equilibrated at 296 K and under 1 atm. View on ac, bc and ab plans.

atom type; the Lorentz-Berthelot mixing rule is employed for two dissimilar non-bonded atoms:

$$\sigma_{ij} = \frac{\sigma_{ii} + \sigma_{jj}}{2};\ \epsilon_{ij} = \sqrt{\epsilon_{ii} + \epsilon_{jj}} \tag{3}$$

The electrostatic contribution is described by the Coulomb potential for:

$$U^{Coul} = \frac{e^2}{4\pi\epsilon_0} \sum_{i \neq j} \frac{q_i q_j}{r_{ij}} \tag{4}$$

where q_i is the partial charge of a particle i, e is the elementary charge, and $\epsilon_0 = 8.85419 \times 10^{-12}$ F/m is the dielectric permittivity of vacuum. Table 1 shows the nonbonded parameters and partial charges. To ensure the electroneutrality of the shlykovite, we reparametrize the partial charges of the O_h and O, as shown in table 1.

Water is modeled using the extended simple-point charge (SPC/E) water model [23]. This water model is made flexible using the parameters provided in ClayFF [14] for 2-body and 3-body interactions. Bonded interactions are only defined for water molecules and hydroxides. The bond (2-body) and angle (3-body) interactions are described by harmonic potentials, respectively:

$$U^{Bond}(r_{ij}) = k_b \left(r_{ij} - r_0\right)^2;\ \ U^{Angle}(\theta_{ij}) = k_a \left(\theta_{ij} - \theta_0\right)^2 \tag{5}$$

where k_b and k_a are the rigidity of the bond and angle, respectively; r_0 and θ_0 are the equilibrium distance and angle, respectively. Table 2 shows the bonded parameters used in ClayFF based on SPC/E water model [23].

The parameters employed to describe the interactions involving K and Na are taken from the respective aqueous ions in ClayFF. Long-range electrostatic interactions are accounted for using Ewald summation methods with precision in terms of forces of 10^{-5}. Tail corrections are used to cope with long-range van der Waals interactions. Simulation are performed with LAMMPS [24]. All simulations are run using periodic boundary conditions.

Table 1: Non-bonded parameters and partial charges. * Reparametrization proposed in this work.

Species and Symbol	partial charge [e]	ϵ_{LJ} [kJ/mol]	σ_{LJ} [Å]
water hydrogen, H_w	0.4238	-	-
water oxygen, O_w	-0.8476	0.650	3.166
hydroxyl hydrogen, H_H	0.425	-	-
hydroxyl oxygen, O_H	-0.95	0.650	3.166
oxygen, O	-1.105*	0.650	3.15
silicon (tetr.), Si	2.1	7.701×10^{-6}	3.302
calcium (oct.), Ca	1.36	2.104×10^{-5}	2.872
sodium, Na	1	0.5443	2.350
potassium, K	1	0.4184	3.334

Table 2: SPC/E water [23]: Bonded parameters .

	k_b [kJ/mol]	r_0 [Å]
O_w-H_w	2318.500	1.0
O_H-H_H	2318.500	1.0
	k_a [kJ.mol^{-1}.rad^{-2}]	θ_0 [°]
H_w -O_w-H_w	191.50	109.47

2.3. Molecular simulations

Molecular dynamics simulations in the isothermal-isobaric ensemble (NσT) are carried out to get the relaxed structure of Na- and K-shlykovite and to compute hydration energies under controlled water content and temperature. In these simulations, the simulation box is allowed to change according to all directions (so that a, b, and c lattice parameters can assume their equilibrium values).

Hybrid GCMC-NVT and GCMC-NσT simulations were carried out to simulate systems under either controlled volume or controlled stress, respectively; in both cases, the water content was allowed to fluctuate in response to an imposed chemical potential. During the GCMC stage, the exchange of water molecules with an infinite water reservoir at imposed chemical potential and temperature is allowed. For temperatures closer to ambient temperatures, one may assume an ideal gas behavior for water since the temperature is well below the critical point for water [25]. The chemical potential of water can be computed from the relative humidity ($RH = P/P_0$, where P is the bulk water pressure and P_0 is the bulk saturating vapor pressure) to be imposed using $\mu - \mu_0 \approx k_B T ln(RH)$, where k_B is the Boltzmann constant, and T is the temperature. In the supporting information, we show that GCMC-NσT simulation of bulk SPC/E water is consistent with the equation of state of this water model. We impose a pressure P in the NσT stage, with the stress tensor $\sigma = -P\mathbf{I}$ where $\mathbf{I}$ is the identity second rank tensor. The six dimensions associated with the (symmetric) stress tensor are controlled independently using their corresponding stress components as the driving forces.

In GCMC-NVT simulation, the variations of volume were imposed by changing the basal spacing. Based on the resolved structures provided by Zubkova et al. [19], we simulate two layers. No specific constraints are imposed on the corresponding two interlayer pores. Thus, the thickness of each interlayer pore can evolve independently during the simulations. The reaction coordinate in this case is preliminarily fixed as twice the basal spacing. Evidence from GCMC-NσT simulation shows that the volume changes in shlykovite are due

Table 3: Lattice parameters, volume V and density ρ of K-, Na-, Li- and Cs-shlykovite obtained from NσT simulations at 296 K and 1 atm: comparison against experimental data from data from Zubkova et al. [19] for (K-)shlykovite.

	(K-)Shlykovite (Exp.) Zubkova et al. [19]	Na-Shlykovite NσT	K-Shlykovite NσT
a [Å]	6.4897	6.35 ± 0.05	6.40 ± 0.04
b [Å]	6.6669	6.92 ± 0.04	6.90 ± 0.04
c [Å]	26.714	24.89 ± 0.61	27.29 ± 0.30
α [°]	90	90.0 ± 3.8	90.0 ± 2.4
β [°]	94.697	89.9 ± 3.6	91.6 ± 5.6
γ [°]	90	90.0 ± 1.0	90.0 ± 0.7
V [Å^3]	1209.12	1089 ± 25	1200 ± 14
ρ [g/cm^3]	2.244	2.38 ± 0.05	2.25 ± 0.03

to changes along c-direction (a and b being unaffected), as in other layered materials [8, 9]. The criterion for convergence of simulations is a stable total energy with a coefficient of variation below 0.4% (see Supporting Information for details).

Nosé-Hoover thermostat with damping parameters of 100 timesteps was used in NVT and NσT simulations. Nosé-Hoover barostat with damping parameters of 1000 timesteps was used in NσT simulations.

3. Results and discussion

3.1. Structural data

Table 3 shows the lattice parameters, volume, and density obtained in an NσT simulation at 296 K and under 1 atm. The NσT results are consistent with the experimental data provided by Zubkova et al. [19], referring to the K-shlykovite. The volume, a and c lattice parameter follows the sequence of cation size (Na < K), whereas b remains approximately constant irrespective of the cation.

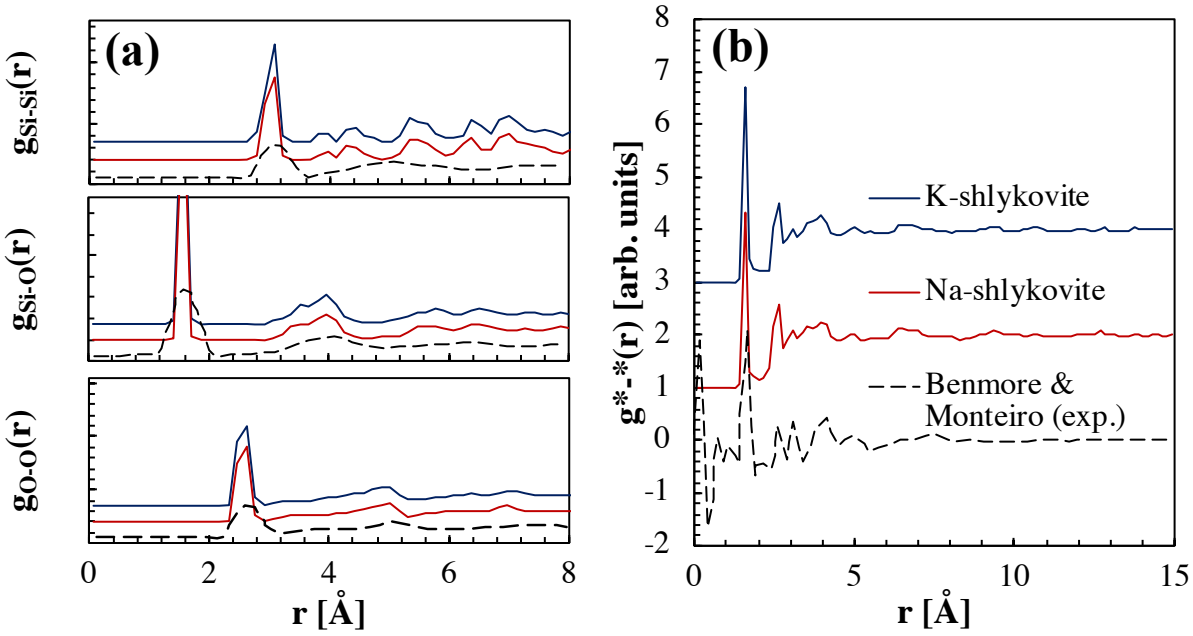

Figure 2: Radial distribution functions (RDF) $g_{i-j}(r)$ of (a) pairs i and j and (b) total pair distribution functions $g_{*-*}(r)$ obtained from molecular simulations on Na- and K-shlykovite at 300 K and under 1 atm compared to the experimental results of Benmore and Monteiro [26] on ASR gels. The curves were shifted to improve the readability.

In Fig. 2, we compare the structure obtained from molecular simulations on Na- and K-shlykovite at a constant number of water molecules n=3 per $Ca[Si_4O_9(OH)]$ with the experimental results of Benmore and Monteiro [26] on ASR gels. To obtain the RDFs, the structures were relaxed at 300 K and under 1 atm in an NσT simulation. The total RDF is in agreement with the experimental results. The first peaks in Si-O and O-O RDFs are associated with SiO_4, which are by design, well reproduced by the ClayFF. The fair agreement observed in the second peaks in these RDFs corroborates the similarity of shlykovite and ASR products. The RDFs of Si-Si pairs obtained from simulations of crystalline systems exhibit a higher frequency of peaks resulting from the ordered structure of shlykovite, whereas a more disordered structure is, as expected, observed in ASR gels obtained from real concrete structures.

3.2. Systems controlled on the water content: hydration energy and volume changes

We study the mechanism of water incorporation in shlykovite using the concept of hydration energy $\Delta U_H(n)$, which has been deployed to study swelling clays [27, 28] and kanemite[13]:

$$\Delta U_H(n) = \frac{\langle U(n)\rangle - \langle U(n_{ref})\rangle}{n} \tag{6}$$

where $\langle U(n)\rangle$ is the ensemble-averaged potential energy computed from MD simulation in which n water molecules (here, normalized per $Ca[Si_4O_9(OH))]$, and including both intra- and interlayer water) are present; and n_{ref} is the water content of reference. We adapt the original definition of $\Delta U_H(n)$ [27], in which n_{ref} =0 (i.e. the reference system is completely dehydrated), to our system in which n includes intralayer water that remain stable [15]. Our reference state is a system with no interlayer water but with intact intralayer water (n_ref =2 per $Ca[Si_4O_9(OH)]$). Note that in the computations of $\Delta U_H(n)$ the system is controlled on the water content n. The hydration energy provides information on the energy associated with water-ion and water-layer interactions as well as layer-layer and ion-layer interactions [27].

To compute the energy of hydration, we perform a simulation of a high-pressure induced hydration process (see the Supporting Information for the details) to get a system with water contents up to n =9.75 water molecules per $Ca[Si_4O_9(OH)]$. To get water contents for n <3, a random interlayer water molecule was deleted (the number of intralayer water molecules was kept constant since the experimental data suggest stability of intralayer water [15]). The system is then sampled in an NσT simulation to get the average volume and cell parameters. Figure 3(a) shows how the volume of Na- and K- changes as a function of n. As expected for a layered mineral stacked along c-axis, the main contribution in the volume change comes from c changes, as can be seen in the comparison of Figs. 4 (a) and (b) (we also report in Appendix A.1 the a and b parameters). The inset shows the volumetric strain $\epsilon_V = (V - V_0)/V_0$

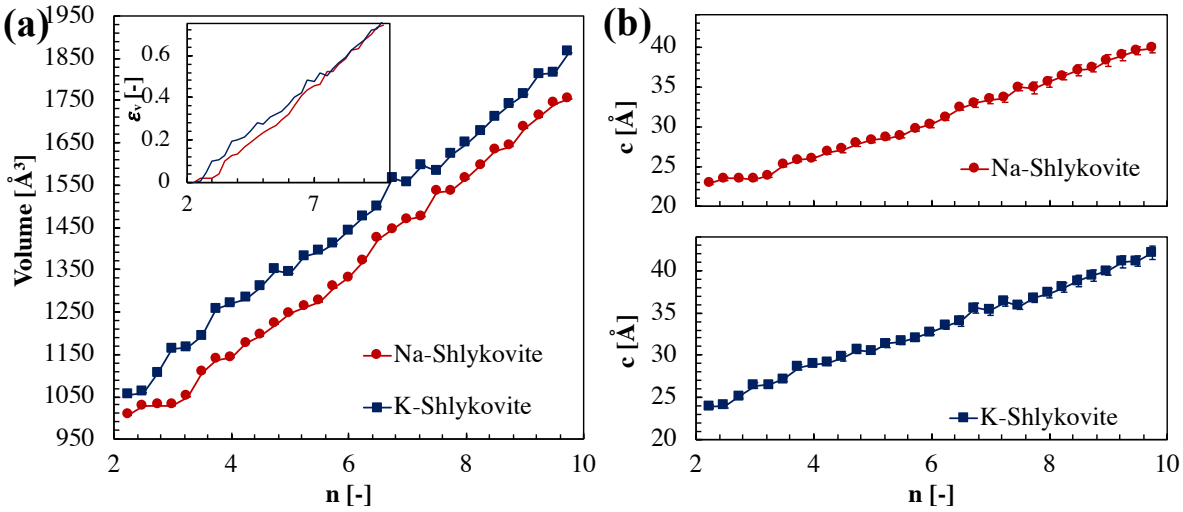

Figure 3: Systems controlled on the water content (number of water molecules n (per $Ca[Si_4O_9(OH)]$)) under 1 atm and 296 K: (a) cell volume and (b) c parameter for Na- and K-shlykovite. The inset in (b) shows the volumetric deformation $\epsilon_V = (V - V_0)/V_0$, with V_0 being the reference volume at n=2.

with respect to the dehydrated state (n =0). Each gain of one water molecule n per $Ca[Si_4O_9(OH)]$ can be associated with a volume increase of roughly 10% in c direction.

The analysis of hydration energies enables us to analyze the propensity of shlykovite to incorporate water. The more negative the value of $\Delta U_H(n)$, when compared to the energy of bulk water, the larger the thermodynamics force to incorporate water in the interlayer. Figure 4 (a) shows the energies of hydration for Na- and K-shlykovite as a function of the number of water molecules n at 296 K and under 1 atm. Contrary to kanemite [13], in shlykovite, K substitutions lead to more negative hydration energy than Na substitutions. For both Na- and K-shlykovite, the hydration energy is comparable to the bulk water energy for n¿6. Being more negative that bulk SPC/E value, the hydration states with n=3 and 5.75 are thermodynamically favored in Na-shlykovite, while the hydration states with n¡6 are favored in K-shlykovite. In both cases, the smaller favored values of n results in more negative hydration energies, which suggest

that the hydration states with lower water content (n =3 for Na-shlykovite and n¡3 for K-shlykovite) are more stable.

The oscillations in the hydration energy curves are an indication of multistability. Multistability resulting in non-convex energy profiles has been identified in other phyllosilicates [7, 8] and have been reported as a key phenomenon at the origin of the thermomechanical behavior of clays [29, 30, 31]. The analysis of the energies barrier in-between stable hydration states can inform on the propensity of the system to exhibit metastability. These aspects will be considered in detail with GCMC-NVT simulations under water-saturated conditions.

We also provide the estimates of the the isosteric heat of hydration (i.e. the negative of the differential enthalpy of hydration) using a finite differences approach [27]:

$$q_{st}(\bar{n}) = RT - \frac{\langle U(n')\rangle - \langle U(n'')\rangle}{n' - n''} \tag{7}$$

where R is the gas constant and $\bar{n} = (n' + n'')/2$, where n' and n'' are two water content in a sequence to which the finite different is applied. The enthalpy of vaporization of SPC/E water is 49.33 kJ/mol (the experimental value is 44.01 kJ/mol) [32]. A q_{st} larger than water enthalpy of vaporization indicates a thermodynamic driving force for further hydration upon the equilibration [27]. On the other hand, a q_{st} smaller than the water enthalpy of vaporization points out to a driving force for dehydration. The results in Figure 4 corroborates that the system is prone to multistability.

3.3. System controlled on the RH: sorption isotherms and volume stability

The sorption isotherms obtained from GCMC-NσT simulation are reported in Fig. 5 for 296 K. We have simulated desorption from an RH of 100% to 1% and adsorption from an RH of 20% up to 100%. In the simulation, we have considered a 6x6x1 system, which yields similar results to simulation with a smaller system (see the supporting information for details). Data from the system equilibrated at RH of 100% have been used as initial configurations in all desorption simulations. Data from the system equilibrated at RH of 20% have

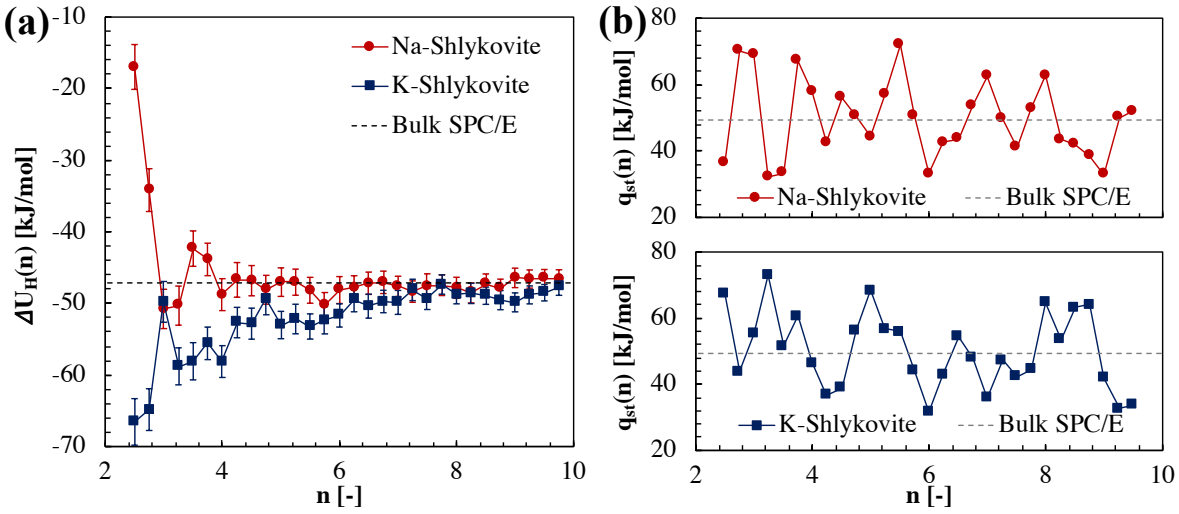

Figure 4: (a) Energies of hydration, and (b) isosteric heat of hydration for Na- and K-shlykovite obtained from MD simulation at NσT ensemble as a function of the number of water molecules n (per $Ca[Si_4O_9(OH)]$) at 296 K and under 1 atm. The respective energies of associated with bulk SPC/E are shown in (a) and (d) for comparison.

been used as initial configurations in all adsorption simulations. We observe that Na-shlykovite exhibits a higher water content than K-shlykovite, which is in agreement with the trends observed experimentally for RH<80%. The water content observed in the simulation remains stable in the range of RH of 10% up to 100%. The experimental results of Shi et al. on Na- and K-shlykovite shows an increase of the water uptake with the RH. It is noteworthy that the DVS method measures the water content without direct differentiation whether the water is taken up in the interlayer or on the powder surface [15]. Powder XRD conducted by the same authors shows that the basal spacing of Na- and K-shlykovite remains the same in the wet and dry sample, which indicates volume stability under sorption. In the Fig. 6, we report the sorption-induced volume changes observed in the GCMC-NσT simulations. In agreement with the experimental evidence, both Na- and K-shlykovite show volume stability for RH ranging from 20 to 100%. These observations corroborate that the water uptake observed in the experiments is due to water adsorption on the surface

and larger pores of the particles of shlykovite [15] and not to interlayer water uptake.

Both Na- and K-shlykovite exhibit stability in a- and b directions, even at low RH. As expected for a layered mineral, changes along c-direction are the main contributors to the volume changes observed especially fo Na-shlykovite at low RH. Note that K-shlykovite exhibits a volume of the unit cell significantly larger than Na-shlykovite, which is expected since K^+ ions are larger than Na^+ ions. Comparing these results with the discussion of the previous section, the energy of hydration for the system with potassium is more negative than that of the system with sodium, as shown in (Fig. 4(a)), but it also favors lower water contents (e.g. for K-shlykovite, the hydration energy is more negative at n=2.25). In contrast, the hydration energy of Na-shlykovite reaches its minimum at n=3. These observations agree with the sorption isotherms in Fig. 5.

The results in this section suggest that shlykovite does not swell as clay minerals such as montmorillonite. ASR damage in the presence of crystalline products should be therefore attributed to other mechanisms.

3.4. System controlled on the volume: evidence of multistability and effective interactions

In this section, we dissect the molecular interactions in Na- and K-shlykovite under controlled volume. The goal is to identify the stable basal spacings in (liquid) water-saturated conditions and to provide effective interactions that can be used in mesoscale simulations (for example of crystallization processes of ASR gels).

In nanolayered materials, the confinement pressure in drained conditions is related to the thermodynamic potential[30, 8]

$$\Lambda(V,T,\mu_w)/A = (F-\mu_w N_w)/A = \Lambda_0(d_0,T,\mu_w)/A - \int_{d_0}^{d} P d(d) \qquad (8)$$

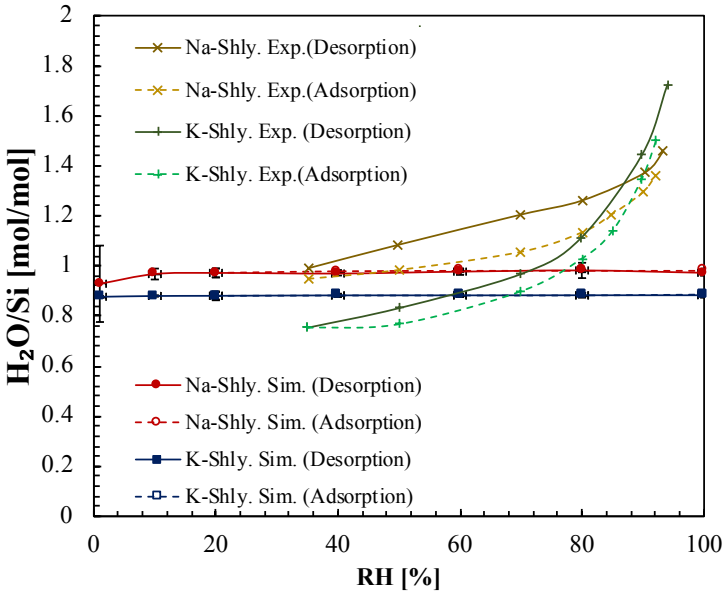

Figure 5: System controlled on the RH: sorption isotherms obtained from GCMC-NσT and volume stability at 296 K and pressure of 1 atm (in NσT stage) for Na- and K-shlykovite. For comparison, we show the isotherms reported by Shi et al. [15] obtained by DVS. To be consistent with the experimental results, hydroxide groups in the shlykovite layer were accounted for in the computations of the water content. Full line denote desorption, Dashed lines denote adsorption.

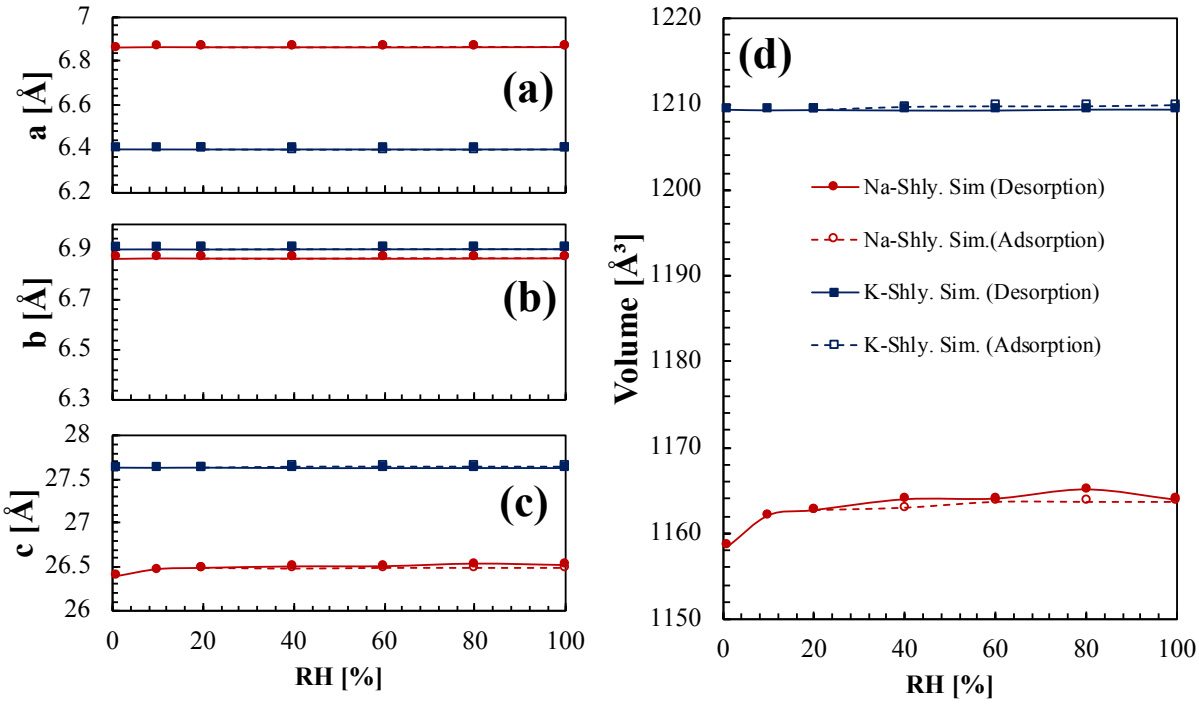

Figure 6: System controlled on the RH: volume stability and anisotropy for Na- and K-shlykovite at 296 K. (a)-(c) lattice parameters and (d) volume of the unit cell volume under sorption for Na- and K-shlykovite at 298 K.

via the expression

$$P = -\frac{1}{A}\left.\frac{\partial \Lambda}{\partial d}\right|_{T,\mu_w} \tag{9}$$

where F is the Helmholtz free energy, A is the surface area of the layer, and d_0 is a basal spacing of reference (associated with a free energy Λ_0). Here, we consider two shlykovite layers, so the reaction coordinate d is given in terms of the c length. The GCMC-NVT simulation, as described in the Models and Methods section, minimizes $\Lambda(V, T, \mu_w)$ [30, 8]. Thus, from the simulation, other than the free energy Λ, we can compute the water content and the disjoining pressure $\Pi = P - P_w$ (i.e the difference between the confining pressure and the fluid pressure $\Pi = P - P_w$), as shown for Na- and K-shlykovite in Fig. 7 for a system at 296 K and under an imposed water pressure $P_W(\mu_W)$ of 1 atm. The equilibrium d_{eq} can be identified as the minimum in the energy profiles. Table 4 reports d for the global minimum. The energy increases steeply with the decrease along with the reaction coordinate for $d < d_{eq}$ due to steric repulsion. The interaction goes to zero for d exceeding approximately 5 nm. The insets in the disjoining pressure and free energy profiles show evidence of the multistability, which is well pronounced for Na-shlykovite.

The profiles in Fig. 7 also informs on the (e.g. [33]):

- Cohesive pressure $P_{co} = min\Pi(d)$: the pressure needed to disjoin two solid layers, which corresponds to the global minimum in the pressure isotherms.

- Surface energy $\gamma_s = -1/(2A)\int_{d_{eq}}^{\infty} Pd(d)$: the energy required to separate two layers placing them infinitely apart.

The values computed for Na- and K-shlykovite are also shown in Table 4. The equilibrium distance in K-shlykovite is larger than in Na-shlykovite, which is expected since the radius of potassium is larger than sodium's. The cohesive pressures are similar for both cases. The surface energy for Na-shlykovite is slightly larger than for K-shlykovite.

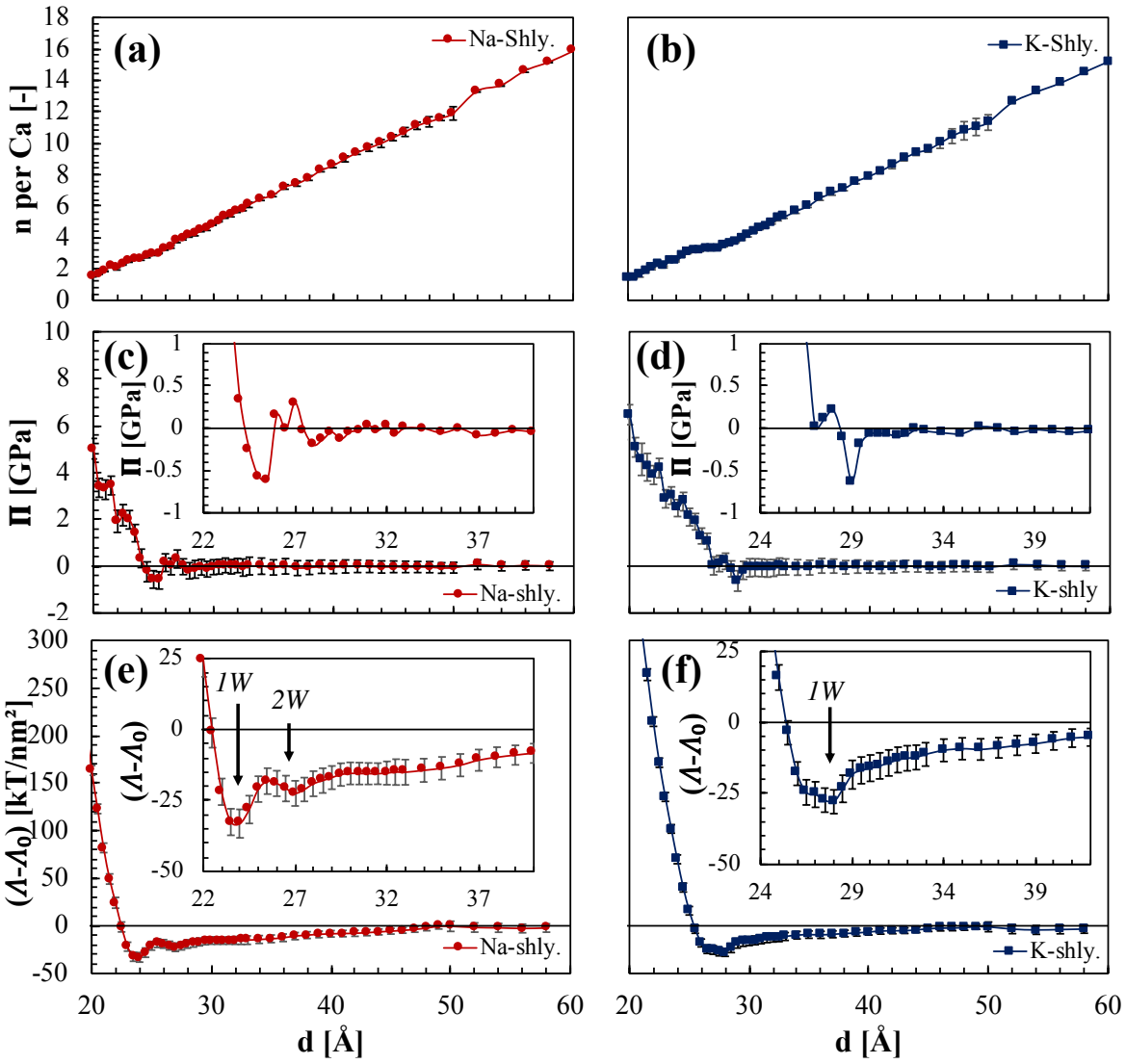

Figure 7: System controlled on the RH: (a)-(b) water content, (c)-(d) disjoining pressure Π and (e)-(f) free energy Λ profiles as a function of the basal spacing for Na- and K-shlykovite (left and right, respectively) at 296 K and under an imposed water pressure $P_W(\mu_W)$ of 1 atm. The insets in (c)-(f) zoom in the oscillatory portions of the pressure and energy profiles.

Table 4: Cohesive pressure P_{co}, and surface energy γ_s of K- and Na-shlykovite at the equilibrium c-length d_{eq} (=arg Min Λ) at 296 K and RH of 100%. Since we simulate two shlykovite layers d_{eq} can be read as twice the equilibrium basal distance.

	Na-shlykovite	K-shlykovite
d_{eq} [Å]	24.3	28.1
P_{co} [GPa]	0.61	0.63
γ_s [J/m^2]	0.064	0.050

Figure 8 shows the effective intermolecular interactions (or Potential of Mean Force, PMF) based on the free energy Λ. We fit the PMF using Mathematica. The fits can be used in future works to study ASR gel (meso)structuration. To capture the oscillation in the energy profiles, we use an expression based on the generalized Lennard-Jones potential plus damped cosine and squared-cosine terms to fit the PMF:

$$U^{PMF}(r_{ij}) = U^{G}_{LJ}(r_{ij}) + A_1 \cos\left[\frac{r_{ij}-B_1}{C_1}\right] e^{-\frac{r_{ij}}{D_1}} + A_2 \cos\left[\frac{r_{ij}-B_2}{C_2}\right]^2 e^{-\frac{r_{ij}}{D_2}} \tag{10}$$

with $U^{G}(r_{ij}) = 4A_0\left[\left(\frac{B_0}{C_0-D_0 r_{ij}}\right)^{2E_0} - \left(\frac{B_0}{C_0-D_0 r_{ij}}\right)^{E_0}\right]$. Table 5 gathers the fitting parameters of the PMF using Eq. 10. The standard error computed for the non-linear fits are shown in the parenthesis.

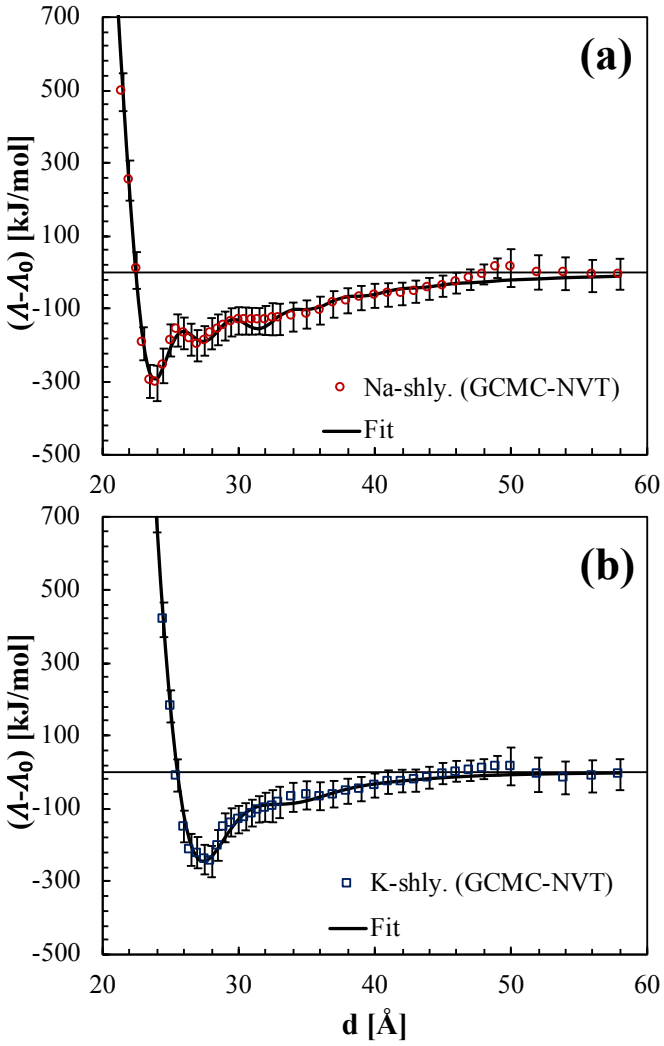

Figure 8: Effective intermolecular interactions: data for mesoscale simulations on Na- and K-shlykovite at 296 K and under an imposed water pressure $P_W(\mu_W)$ of 1 atm and fittings using Eq. 10.

Table 5: Fitting parameters of the PMF using Eq. 10. The standard error associated with the fits are shown in the parenthesis.

	Na-shlykovite	K-shlykovite
A_0 [kJ/mol]	148.6 (8.9)	253.3 (56.3)
B_0 [Å]	27.0 (2.6)	26.1 (7.3)
C_0 [-]	8.15 (8.62)	13.5 (14.0)
D_0 [-]	0.80 (0.48)	0.54 (0.91)
E_0 [-]	5.76 (2.58)	11.3 (14.2)
A_1 [kJ/mol]	3.51×10^6 (2.61×10^6)	3.73×10^9 (8.12×10^4)
B_1 [Å]	-45.5 (6.0)	-43.3 (36.2)
C_1 [Å]	1.48 (0.13)	1.47 (0.90)
D_1 [Å]	2.38 (0.20)	1.39 (0.14)
A_2 [kJ/mol]	-9.61×10^3 (8.20×10^3)	6.26×10^6 (1.13×10^7)
B_2 [Å]	15.5 (0.2)	31.9 (0.57)
C_2 [Å]	1.29 (0.03)	2.63 (0.47)
D_2 [Å]	5.45 (1.08)	2.69 (0.42)

4. Conclusion

Nanocrystalline ASR products were modeled using molecular simulation techniques. We studied the intermolecular interactions of these products under controlled conditions in order to better understand the stability of ASR products under RH variations. The main conclusions that can be drawn from our results are:

- *Shlykovite structure with ClayFF provides a sound molecular model of ASR products* that can be used to understand with atomic-detail the nanoscale processes leading to ASR formation. The molecular models are in agreement with experimental evidence regarding the structure and lattice parameters.

- *Water content and volume of shlykovite remain stable for RH ranging from 20 to 100%*. For the system controlled on the water content, we observe that the structure swells to accommodate additional water molecules.

However, the water content on shlykovite does not change significantly in a system under RH control, which is a condition corresponding better to experimental and *in situ* conditions. Our results corroborate that crystalline ASR products do not swell akin to swelling clays minerals as montmorillonite [15].

- *The volume and water content associated with Na- and K-shlykovite systems are significantly different.* Our results corroborate the crucial influence of specific ion effects on the behavior of layered materials. Evidence from glass science shows that mixing sodium and potassium may lead to particular effects [34]. Future work should address these effects as well as take into account other alkalies of interest in cement and concrete applications (such as lithium and cesium).

- *The effective interactions that can be used to model coarser length scales are provided.* The potential of mean force provided is valuable information for mesoscale modeling, contributing to the effort to understand predict and prevent ASR damage. Further analysis, following the theoretical framework proposed in this study, may be carried out in order to better understand the stability of ASR products under temperature and pressure variations [35].

Appendix A Details on molecular simulations of Na- and K-shlykovite

A.1 Pressure-induced hydration process

To compute the energy of hydration at higher water contents, we perform a simulation forcing the ingress of water within the shlykovite structure. To do so, a GCMC simulation with high pressure of water reservoir (P_w= 1.0 GPa) is performed. The pressure required to induce hydration in microporous materials is generally on the order of a few gigapascals (e.g. [36]). The simulations were stopped once the water content exceeded n =9.75 water molecules per $Ca[Si_4O_9(OH)]$ since we were not interested in the equilibrium water content at

higher water pressures. Water ingress occurs within interlayer space; intralayer water content remains stable during the pressure-induced hydration process. The a and b lattice parameters remain stable during the process as depicted in Fig. 9.

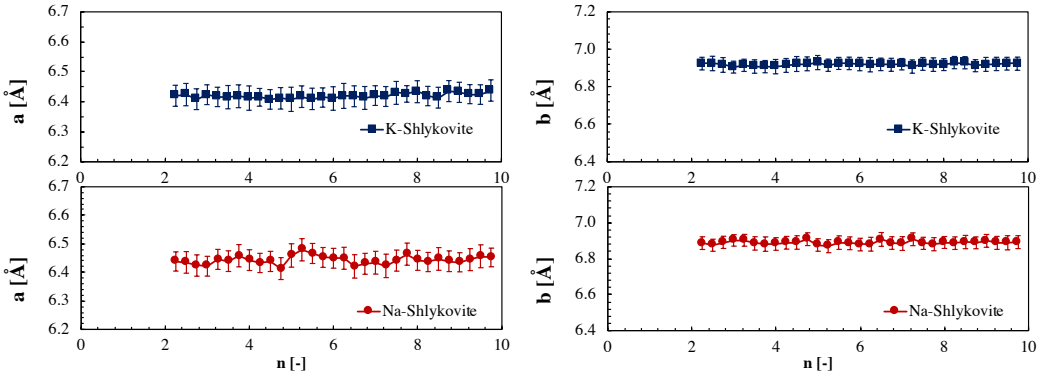

Figure 9: a and b lattice parameter of Na- and K-shlykovite in a system controlled on the water content (number of water molecules n (per $Ca[Si_4O_9(OH)]$)) under 1 atm and 296 K.

A.2 Convergence of GCMC simulations

We adopt a convergence criterion in GCMC simulation a stable total energy with a coefficient of variation (CV) below 0.4%. Figure 10 shows the coefficient of variation for the total energy as a function of the reaction coordinate adopted in GCMC simulations. For most of the cases, the CV remains below 0.3%.

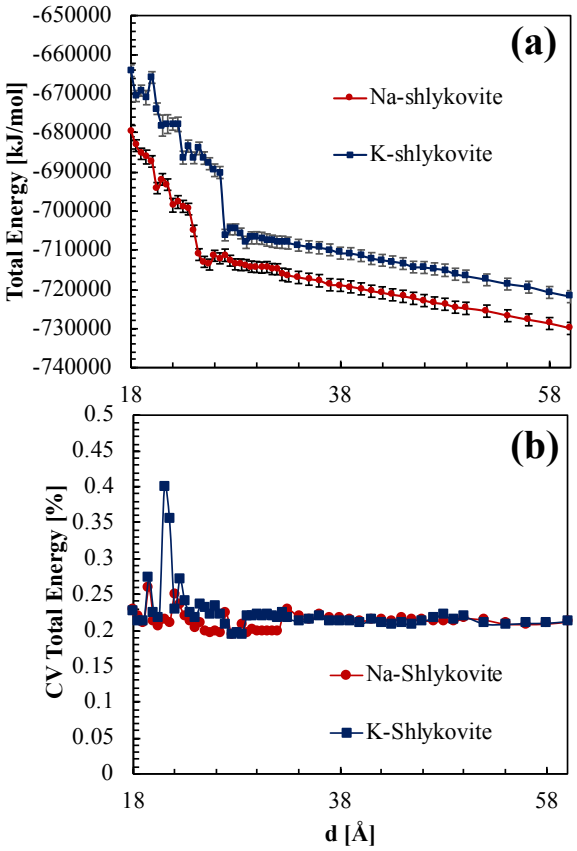

Figure 10: Convergence of GCMC simulations: (a) total energy and (b) coefficient of variation (standard deviations divided by the mean) of the total energy in GCMC simulations as a function of the reaction coordinated d.

A.3 Hybrid GCMC-Nσ T

A.3.1 Hybrid GCMC-NPT of bulk water

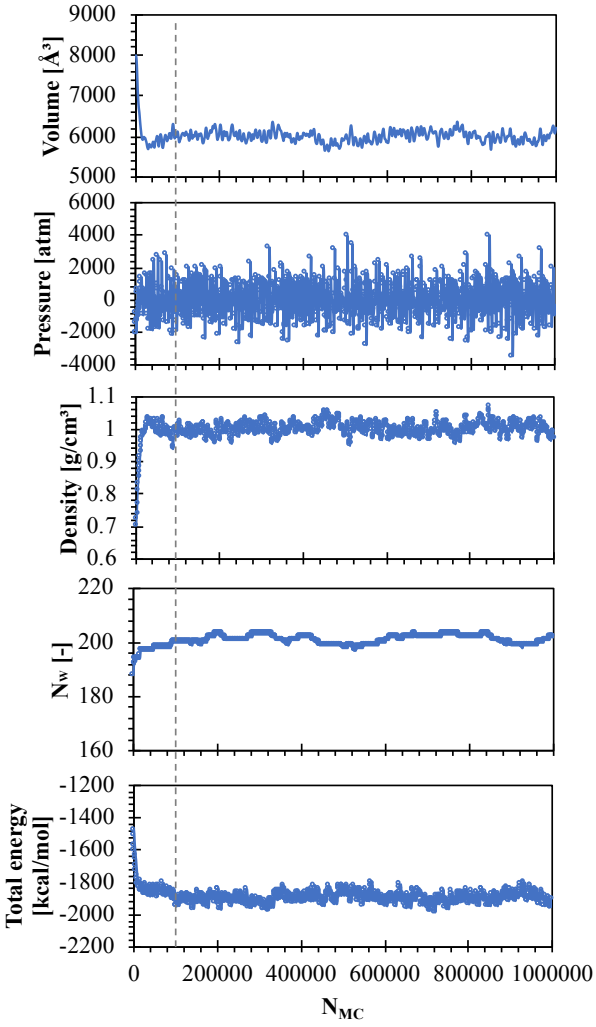

Figure 11: Instantaneous quantities from hybrid GCMC-NPT simulation of bulk SPC/E water at 296 K and under 1 atm as a function of the number of MC steps N_{MC}. We assume that the system is equilibrated after 10000 MC steps.

We use the hybrid GCMC-NPT simulation with imposed hydrostatic pressure (i.e. we couple the three diagonal components together when pressure is

computed) to simulate bulk SPC/E water. The goal is to verify whether the hybrid simulation allows retrieving the expected thermodynamic properties of bulk water. Figure 11 shows the instantaneous quantities (volume, pressure, density, number of water molecules N_w and total energy) from hybrid GCMC-NPT simulation of bulk SPC/E water at 296 K and under 1 atm as a function of the number of MC steps N_{MC}. We assume that the system is equilibrated after 10000 MC steps. We compute the average of densities for $N_{MC}¿10000$ and we find a density of 1.000 $\pm$ 0.019 g/cm^3 at 296 K and under 1 atm. This result is consistent with the values reported for the SPC/E water model. For example, at 300K and under 10^{-4} GPa, the density reported for SPC/E water is 1.000 g/cm^3 and the experimental value is 0.996 g/cm^3 [37].

A.3.2 Size effects on desorption isotherms

Figure 12 shows the desorption isotherms for Na- and K-shlykovite system with different sizes: 2x2x1 and 6x6x1 unit cells. No size effects were identified at this scale for K-shlykovite: 2x2x1 and 6x6x1 isotherms superpose. Na-shlykovite is more prone to exhibit size effects at the molecular scale. In the main text, we have reported only 6x6x1 systems since the corresponding results are expected to be more accurate.

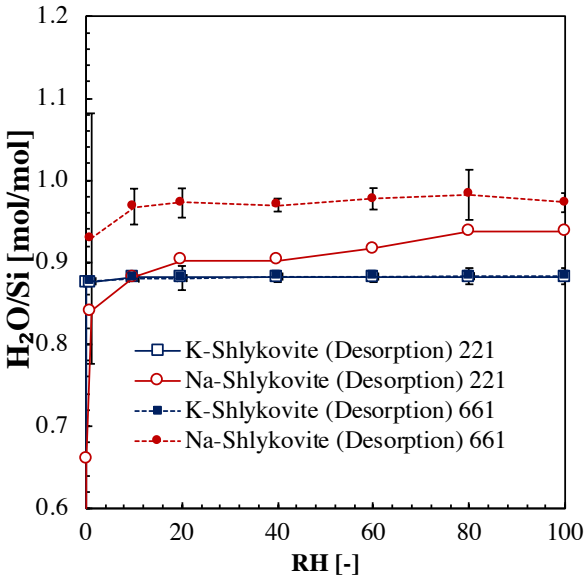

Figure 12: Size effects in GCMC-NσT simulations.

References

[1] L. S. Dent Glasser, N. Kataoka, The chemistry of 'alkali-aggregate' reaction, Cement and Concrete Research 11 (1) (1981) 1–9.

[2] F. Rajabipour, E. Giannini, C. Dunant, J. H. Ideker, M. D. A. Thomas, Alkali–silica reaction: Current understanding of the reaction mechanisms and the knowledge gaps, Cement and Concrete Research 76 (2015) 130–146.

[3] A. Leemann, T. Katayama, I. Fernandes, M. A. T. M. Broekmans, Types of alkali–aggregate reactions and the products formed, Proceedings of the Institution of Civil Engineers - Construction Materials 169 (3) (2016) 128–135.

[4] T. E. Stanton, Expansion of Concrete through Reaction between Cement and Aggregate, 1940.

[5] E. S. Boek, P. V. Coveney, N. T. Skipper, Molecular Modeling of Clay Hydration: A Study of Hysteresis Loops in the Swelling Curves of Sodium Montmorillonites, Langmuir 11 (12) (1995) 4629–4631.

[6] E. J. M. Hensen, B. Smit, Why Clays Swell, The Journal of Physical Chemistry B 106 (49) (2002) 12664–12667. doi:10.1021/jp0264883.
URL https://pubs.acs.org/doi/10.1021/jp0264883

[7] T. J. Tambach, P. G. Bolhuis, E. J. M. Hensen, B. Smit, Hysteresis in Clay Swelling Induced by Hydrogen Bonding: Accurate Prediction of Swelling States, Langmuir 22 (3) (2006) 1223–1234.

[8] T. Honorio, L. Brochard, M. Vandamme, Hydration Phase Diagram of Clay Particles from Molecular Simulations, Langmuir 33 (44) (2017) 12766–12776.

[9] T. Honorio, Monte Carlo Molecular Modeling of Temperature and Pressure Effects on the Interactions between Crystalline Calcium Silicate Hydrate Layers, Langmuir 35 (11) (2019) 3907–3916.

[10] E. S. Boek, P. V. Coveney, N. T. Skipper, Monte Carlo Molecular Modeling Studies of Hydrated Li-, Na-, and K-Smectites: Understanding the Role of Potassium as a Clay Swelling Inhibitor, Journal of the American Chemical Society 117 (50) (1995) 12608–12617. doi:10.1021/ja00155a025.
URL https://pubs.acs.org/doi/abs/10.1021/ja00155a025

[11] E. Ferrage, B. A. Sakharov, L. J. Michot, A. Delville, A. Bauer, B. Lanson, S. Grangeon, G. Frapper, M. Jiménez-Ruiz, G. J. Cuello, Hydration Properties and Interlayer Organization of Water and Ions in Synthetic Na-Smectite with Tetrahedral Layer Charge. Part 2. Toward a Precise Coupling between Molecular Simulations and Diffraction Data, The Journal of Physical Chemistry C 115 (5) (2011) 1867–1881. doi:10.1021/jp105128r.
URL http://dx.doi.org/10.1021/jp105128r

[12] B. F. Ngouana W., A. G. Kalinichev, Structural Arrangements of Isomorphic Substitutions in Smectites: Molecular Simulation of the Swelling Properties, Interlayer Structure, and Dynamics of Hydrated Cs–Montmorillonite Revisited with New Clay Models, The Journal of Physical Chemistry C 118 (24) (2014) 12758–12773. doi:10.1021/jp500538z.
URL http://dx.doi.org/10.1021/jp500538z

[13] R. J. Kirkpatrick, Experimental and molecular dynamics modeling studies of interlayer swelling: water incorporation in kanemite and ASR gel, Materials and Structures 38 (278) (2005) 449–458.

[14] R. T. Cygan, J.-J. Liang, A. G. Kalinichev, Molecular Models of Hydroxide, Oxyhydroxide, and Clay Phases and the Development of a General Force Field, The Journal of Physical Chemistry B 108 (4) (2004) 1255–1266.

[15] Z. Shi, G. Geng, A. Leemann, B. Lothenbach, Synthesis, characterization, and water uptake property of alkali-silica reaction products, Cement and Concrete Research 121 (2019) 58–71.

[16] Z. Shi, A. Leemann, D. Rentsch, B. Lothenbach, Synthesis of alkali-silica reaction product structurally identical to that formed in field concrete, Materials & Design (2020) 108562doi:10.1016/j.matdes.2020.108562.
URL http://www.sciencedirect.com/science/article/pii/S0264127520300952

[17] R. J. Prado, F. Tiecher, N. P. Hasparyk, D. C. C. D. Molin, Structural characterization of alkali-silica reaction gel: An x-ray absorption fine structure study, Cement and Concrete Research 123 (2019) 105774.

[18] G. Geng, Z. Shi, A. Leemann, C. Borca, T. Huthwelker, K. Glazyrin, I. V. Pekov, S. Churakov, B. Lothenbach, R. Dähn, E. Wieland, Atomistic structure of alkali-silica reaction products refined from X-ray diffraction and micro X-ray absorption data, Cement and Concrete Research 129 (2020) 105958. doi:10.1016/j.cemconres.2019.105958.

[19] N. V. Zubkova, Y. E. Filinchuk, I. V. Pekov, D. Y. Pushcharovsky, E. R. Gobechiya, Crystal structures of shlykovite and cryptophyllite: comparative crystal chemistry of phyllosilicate minerals of the mountainite family, European Journal of Mineralogy 22 (4) (2010) 547–555.

[20] A. Vollpracht, B. Lothenbach, R. Snellings, J. Haufe, The pore solution of blended cements: a review, Materials and Structures 49 (8) (2016) 3341–3367.

[21] T. Honorio, F. Benboudjema, T. Bore, M. Ferhat, E. Vourc'h, The pore solution of cement-based materials: structure and dynamics of water and ions from molecular simulations, Physical Chemistry Chemical Physics 21 (2019) 11111–11121.

[22] I. V. Pekov, N. V. Zubkova, Y. E. Filinchuk, N. V. Chukanov, A. E. Zadov, D. Y. Pushcharovsky, E. R. Gobechiya, Shlykovite KCa[Si4o9(OH)] · 3h2o and cryptophyllite K2ca[Si4o10] · 5h2o, new mineral species from the Khibiny alkaline pluton, Kola Peninsula, Russia, Geology of Ore Deposits 52 (8) (2010) 767–777.

[23] H. J. C. Berendsen, J. R. Grigera, T. P. Straatsma, The missing term in effective pair potentials, The Journal of Physical Chemistry 91 (24) (1987) 6269–6271. doi:10.1021/j100308a038.
URL http://dx.doi.org/10.1021/j100308a038

[24] S. Plimpton, Fast Parallel Algorithms for Short-Range Molecular Dynamics, Journal of Computational Physics 117 (1) (1995) 1–19.

[25] M. Chen, B. Coasne, R. Guyer, D. Derome, J. Carmeliet, Role of hydrogen bonding in hysteresis observed in sorption-induced swelling of soft nanoporous polymers, Nature Communications 9 (1) (2018) 3507. doi:10.1038/s41467-018-05897-9.
URL https://www.nature.com/articles/s41467-018-05897-9

[26] C. J. Benmore, P. J. M. Monteiro, The structure of alkali silicate gel by total scattering methods, Cement and Concrete Research 40 (6) (2010) 892–897.

[27] D. E. Smith, Molecular Computer Simulations of the Swelling Properties and Interlayer Structure of Cesium Montmorillonite, Langmuir 14 (20) (1998) 5959–5967.

[28] J. Wang, A. G. Kalinichev, R. J. Kirkpatrick, X. Hou, Molecular Modeling of the Structure and Energetics of Hydrotalcite Hydration, Chemistry of Materials 13 (1) (2001) 145–150.

[29] T. Honorio, L. Brochard, M. Vandamme, A. Lebée, Flexibility of nanolayers and stacks: implications in the nanostructuration of clays, Soft Matter.

[30] L. Brochard, T. Honório, M. Vandamme, M. Bornert, M. Peigney, Nanoscale origin of the thermo-mechanical behavior of clays, Acta Geotechnica 12 (6) (2017) 1261–1279.

[31] L. Brochard, T. Honório, Revisiting thermo-poro-mechanics under adsorption: Formulation without assuming gibbs-duhem equation, International Journal of Engineering Science 152.

[32] C. Vega, J. L. F. Abascal, Simulating water with rigid non-polarizable models: a general perspective, Physical Chemistry Chemical Physics 13 (44) (2011) 19663.

[33] S. Masoumi, H. Valipour, M. J. Abdolhosseini Qomi, Intermolecular Forces between Nanolayers of Crystalline Calcium-Silicate-Hydrates in Aqueous Medium, The Journal of Physical Chemistry C 121 (10) (2017) 5565–5572.

[34] Y. Yu, M. Wang, M. M. Smedskjaer, J. C. Mauro, G. Sant, M. Bauchy, Thermometer Effect: Origin of the Mixed Alkali Effect in Glass Relaxation, Physical Review Letters 119 (9) (2017) 095501. doi:10.1103/PhysRevLett.119.095501.
URL https://link.aps.org/doi/10.1103/PhysRevLett.119.095501

[35] L. Struble, S. Diamond, Unstable swelling behaviour of alkali silica gels, Cement and Concrete Research 11 (4) (1981) 611–617. doi:10.1016/0008-8846(81)90091-0.
URL http://www.sciencedirect.com/science/article/pii/0008884681900910

[36] S. You, D. Kunz, M. Stöter, H. Kalo, B. Putz, J. Breu, A. V. Talyzin, Pressure-Induced Water Insertion in Synthetic Clays, Angewandte Chemie International Edition 52 (14) (2013) 3891–3895. doi:10.1002/anie.201210060.
URL https://onlinelibrary.wiley.com/doi/abs/10.1002/anie.201210060

[37] C. Vega, C. McBride, E. Sanz, J. L. F. Abascal, Radial distribution functions and densities for the SPC/E, TIP4P and TIP5P models for liquid water and ices Ih, Ic, II, III, IV, V, VI, VII, VIII, IX, XI and XII, Physical Chemistry Chemical Physics 7 (7) (2005) 1450–1456. doi:10.1039/B418934E.
URL https://pubs.rsc.org/en/content/articlelanding/2005/cp/b418934e